MMC–Based Multiport Power Converters

This paper analyzes two modular power converter concepts, based on Cascaded H-Bridges (CHB) and Modular Multilevel Converter (MMC) topologies respectively, with special attention to the second design. Both have common characteristics and can provide the required functionalities for Power Electronic Transformers (PETs). Criteria for their analysis will include aspects like number of required cells, characteristics of the power devices, functionalities and potential uses.

Conventional Line-Frequency Transformers (LFTs) are key elements in transmission and distribution systems to interface the different voltage levels in the grid. LFTs are a well established technology, they are relatively cheap, efficient and reliable. However, they have several limitations, including: voltage drop under load; sensitivity to harmonics, load imbalances and DC offsets; no overload protection and low efficiency when operate with low load levels or no load [1].

PETs, also called Solid State Transformers (SSTs), are envisioned as a semiconductor based alternative to LFTs. PETs are able to provide advanced functionalities such as power flow control, reactive power, harmonics and imbalances compensation, availability of low voltage DC (LVDC) link and smart protection. High switching frequencies of the semiconductors also enable a significant reduction of the volume and weight of the core material [1]-[4].

Generally speaking, PETs are expected to beat the LFTs in terms of power density and much superior functionalities, but would be inferior in terms of cost, efficiency (full load) and reliability. Based on this, there is a number of applications in which the use of PETs can be advantageous compared to standard LFTs. Smart-grid applications require an efficient integration of distributed generation and storage resources, flexible routing mechanisms, active filtering and protection mechanism. While power density might not be a key aspect for onshore applications, it can be of paramount importance for offshore applications [5]. Traction and subsea systems are also examples of space-critical applications in which the improved performances and power density of PETs compared to LFTs can be determinant [6], [7].

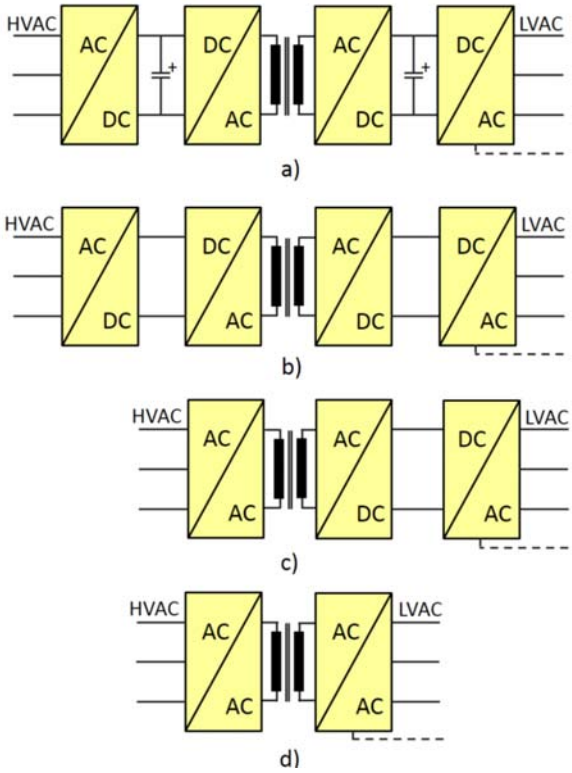

Fig. 1.- 3-phase PET arrangements. a) Fully modular three-stage PET including DC link and back-to-back converters in both HV and LV sides; b) Three-stage PET using indirect matrix converters in both HV and LV sides; c) Two-stage PET using a direct matrix converter in the HV side and indirect matrix converter in the LV side. d) One-stage PET based using direct matrix converter. Note: LVAC port can be either 3 wire or 4 wire.

Practically all PET topologies provide at least a high-voltage AC (HVAC) and a low-voltage AC (LVAC) ports, therefore connecting two AC systems (see Fig. 1). It is noted that the terms HVAC and LVAC are generic and do not necessarily correspond to voltage ranges defined in standards. The general scheme shown in Fig. 1 can be used to realize either an HVAC/MVAC, an MVAC/LVAC or an HVAC/LVAC transformation according to the voltage levels defined e.g. in standard IEC 60038.

PETs topologies in Fig. 1 are seen to consist of three major blocks:

- One (or more) power-converter blocks to transform the grid frequency (low frequency) AC voltage into a high frequency AC voltage.
- A central isolation block using a high frequency transformer.
- One (or more) power-converter block to transform the high frequency AC voltage into a low frequency AC voltage.

A common criterion for the classification of PET topologies is the number of energy conversion stages. PET designs using one, two or three stages have been proposed [5], [8], a fully modular three stage approach (Fig. 1a) appears to be the most popular choice [2], [9]-[11]. This configuration

implies the use of capacitors in the DC links, but this enables a separate design and optimization of each converter stage. Elimination of the DC link capacitors is possible but requires the use of indirect matrix converter topologies (Fig.1b). It is also possible to reduce the number of stages to two (Fig. 1c) or one (Fig. 1d), use of direct matrix converter topologies being required in this case. Matrix based approaches get rid of bulky and lifetime-limited energy-storing capacitors, improving therefore power density and reliability. However, they require the use of a larger number of power devices, introduce constraints in their optimization and complicate the control and protections [5], what has prevented their wide industrial application [12].

One further advantage of the three-stage design shown in Fig. 1 is the presence of DC links both in the HV and LV sides, enabling the inclusion of LVDC and/or HVDC ports in the PET. The resulting multiport topologies can provide additional functionalities, e.g. connection to HVDC transmission systems or the integration of energy storage devices or distributed energy resources (DER) [13], [14]. However, these enhancements can imply an increase of the PET complexity and cost, which needs to be considered.

This paper analyzes two modular PET topologies, namely CHB-based PET [11] and MMC-based PET [15], [16]. Criteria for the evaluation includes number and type of the ports provided by the PET, number of cells and number and rating of power devices. CHB and MMC topologies are introduced first. The resulting PET structures using both concepts are later analyzed. Finally, two examples of application of MMC-based multiport converters are discussed: smart-grid and vessels.

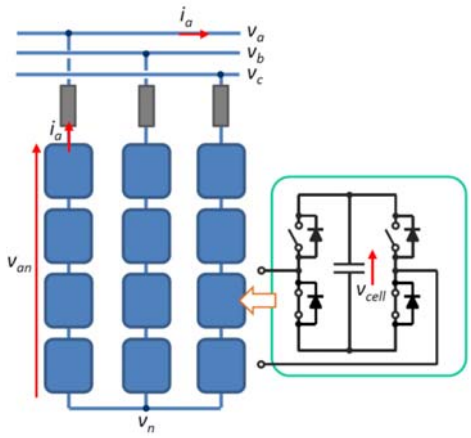

Fig. 2.- Schematic representation of a CHB multilevel converter

CHB and MMC topologies

The CHB converter is a particular case of cascaded converter, based on the series connection of H-bridge cells. A three-phase CHB is shown in Fig. 2. The cells can produce three voltage levels:

v_{cell}, 0 and $-v_{cell}$. By series connection of the N cells in each phase, $2N+1$ levels for the phase voltages and $4N+1$ levels for the phase-to-phase voltages can be obtained. The implementation shown in Fig. 2 does not include a DC voltage source to supply the cell voltage. Due to this, its use would limited to applications which do not involve active power handling, such as reactive power and harmonic compensation. The cells capacitors are maintained at a constant target voltage (average) by the control in this case [17], [18]. Inverter operation (i.e. power conversion between DC and AC ports) of the CHB multilevel converter is possible by feeding each cell from an isolated DC supply, which are normally obtained from multipulse diode rectifiers [19]

The most relevant properties of the CHB topology are:

- High terminal voltages are achieved by just serializing identical cells.
- Voltage sharing among devices is intrinsic to the design, since the voltage blocked by each device is limited to v_{cell}.
- Allows redundancy by simply including spare cells in the legs.
- It shares advantageous features of other multilevel topologies which are derived from the improved output voltage wave shape, e.g. reduced size of AC filters, EMI reduction and lower switching losses thanks to the reduced switching frequency.

One distinguishing characteristic of the CHB topology shown in Fig. 2, compared to other multilevel topologies like the Neutral Point Clamped (NPC) or Flying Capacitor (FC), is that it does not provide an HVDC port.

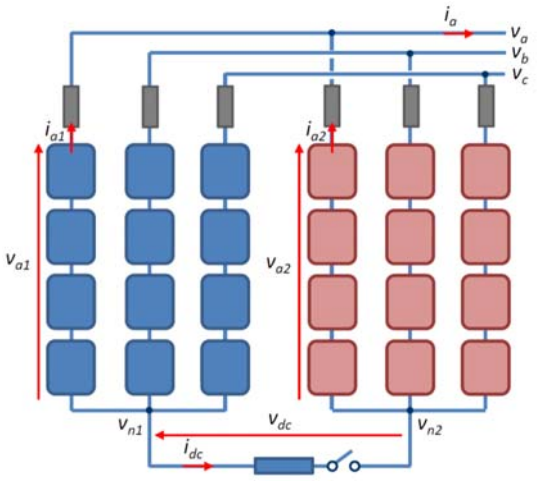

Fig. 3.- Parallel connection of two CHB modular multilevel converters

The MMC can be seen as an evolution of the CHB to provide a DC port [20], [23]-[25]. The DC voltage v_{dc} is obtained between the neutral point of two CHBs connected in parallel, as shown in Fig.

3. The desired DC voltage (2) is produced by adding homopolar voltage components v_{n1} and v_{n2} to the voltage commands of both CHBs (2) and (3). This is graphically shown in Fig. 4.

$$v_{dc}^{*} = v_{n1}^{*} - v_{n2}^{*} \tag{1}$$

$$v_{x1}^{*'} = v_{x1}^{*} + v_{n1}^{*} \qquad \text{with } x = a, b, c \tag{2}$$

$$v_{x2}^{*'} = v_{x2}^{*} + v_{n2}^{*} \tag{3}$$

If a load is now connected between both neutrals, a DC current (i_{dc}) will flow (switch is closed at $t=t_3$ in Fig. 4). Such DC current will add up to the AC currents (i_{a1}; i_{a2}), but will circulate within the converter legs, i.e. it will not show up in the grid current i_a, which remains being purely AC. The grid current i_a is evenly split (ideally) between the two CHBs. The DC current i_{dc} is the so called *circulating current*, and is evenly split (ideally) among all the three phases.

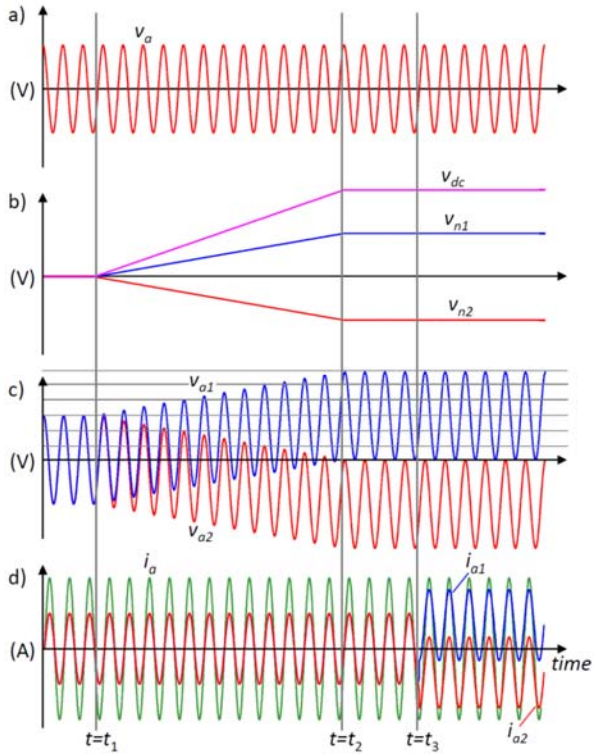

Fig. 4.- Wave shapes for the power converter in Fig. 2. Homopolar voltage injection starts at $t=t_1$ and reaches its steady state value at $t=t_2$. The switch connecting the two neutrals is closed at $t=t_3$

While in the scheme shown in Fig. 3, the DC port is a passive load and therefore can only consume power, the power flow in the DC link can be bidirectional.

The power balance equation of the MMC, neglecting losses and assuming that the cell capacitor voltages remain constant, is given by (4)-(5).

$$P_{ac} = v_a i_a + v_b i_b + v_c i_c \tag{4}$$

$$P_{ac} = P_{dc} = v_{dc} i_{dc} \tag{5}$$

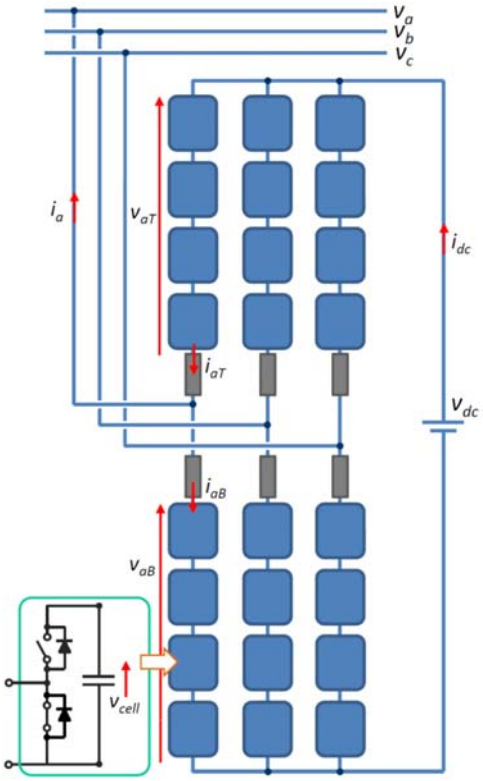

Fig. 5.- Modular Multilevel Converter

Rearranging the two CHBs in Fig. 3, the conventional representation of the MMC is obtained, Fig. 5. The basic equations describing the electric behavior of the MMC (6)-(9) are readily deduced from Fig. 5, where subindexes *T* and *B* stand for the top and bottom arms of the MMC respectively [26]-[34]. . The voltage drop in the arm inductors has been neglected for the sake of simplicity. It is seen from Fig. 4 and (7)-(8) that both arm (and therefore cells) voltages and currents include DC and AC components [26], [27].

$$v_{xT} + v_{xB} = v_{dc} \qquad \text{with } x = a, b, c \tag{6}$$

$$v_{xT} = \frac{v_{dc}}{2} - v_x \quad ; \quad v_{xB} = \frac{v_{dc}}{2} + v_x \tag{7}$$

$$i_{xT} = \frac{i_{dc}}{3} + \frac{i_x}{2} \quad ; \quad i_{xB} = \frac{i_{dc}}{3} - \frac{i_x}{2} \tag{8}$$

A key aspect in the design of the MMC is the ratio between the DC and AC port voltages, which indicates how much of the available DC bus voltage is actually used to produce the AC voltage. This ratio is given by (9) adding triplen harmonics to the phase voltages and increases to (10) (i.e. less margin between v_{dc} and v_a) if triplen harmonics are not used.

$$R_{thi\,(pu)} = \frac{\sqrt{3}\left|v_{a\,(peak)}\right|}{v_{dc}} \tag{9}$$

$$R_{no\,thi\,(pu)} = \frac{2\left|v_{a\,(peak)}\right|}{v_{dc}} \tag{10}$$

Values of R significantly lower than one means that the MMC has a large voltage margin between its DC and AC port voltages, and therefore can operate without violating its voltage limits even in the event of anomalies, e.g. DC voltage lower than expected, or AC voltages larger than expected. This also opens the opportunity to implement redundancy-based fault tolerant designs [35], [36]. However, small values of R also imply a misuse of the cells. On the contrary, values of R closer to one imply a better use of the cells and power devices, but at the price of an increased risk of forcing the MMC to operate without the required voltage safety margin.

Several conclusions can be reached comparing the topologies in Fig. 2 and Fig. 5:

- Because of the injection of homopolar voltages v_{n1} and v_{n2}, phase-to-neutral voltages in the MMC are unipolar but of larger peak value compared to the case without injecting homopolar voltages (see Fig. 4-c). A consequence of this is that for a given AC voltage (v_a; v_b; v_c) and cell voltage (v_{cell}), the MMC requires twice the number of cells per arm, thus, four times the number of cells compared to the CHB. This can be seen as the *price to pay* to obtain the DC link.
- The voltage produced by the CHB cells must be bipolar, full bridges are therefore required (see Fig. 2). On the contrary, the voltage produced by the MMC cells is unipolar. Hence, half bridges can be used in this case (see Fig. 5).
- It is finally noted that the use of full-bridge cells in the CHB design can result in a higher current capability, as two states are now available to bypass the cell (cell voltage equal to zero), enabling a better distribution of the losses.

A comparative analysis between the MMC and CHB topologies in terms of semiconductor requirements, efficiency, cell capacitor sizing, etc. can be found in [37]-[38].

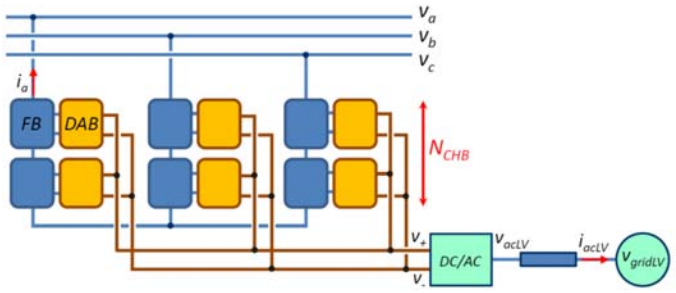

Fig. 6.- CHB-based PET. For the sake of simplicity, inductors connecting the CHB to the grid are not shown

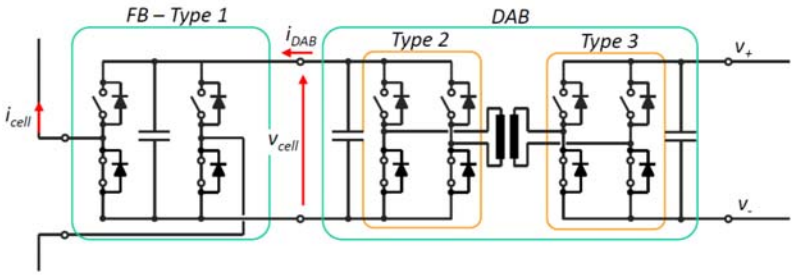

Fig. 7.- CHB cell and DAB for the CHB-based PET

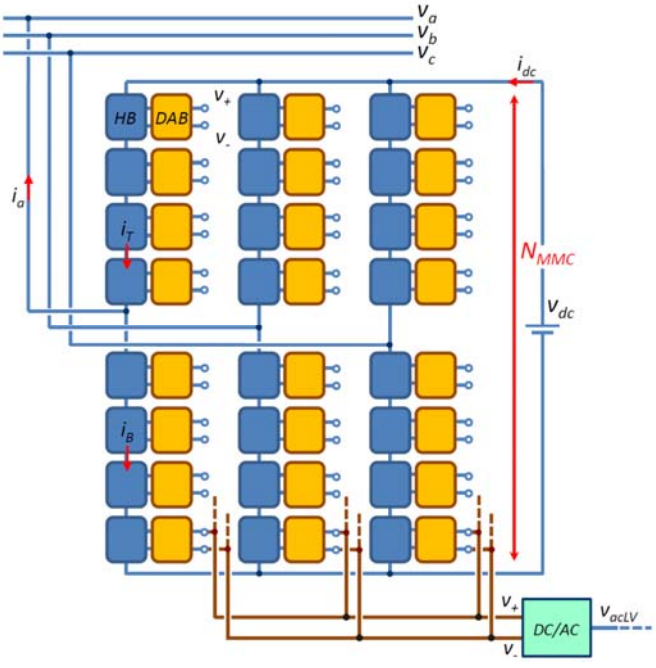

Fig. 8.- MMC-based PET

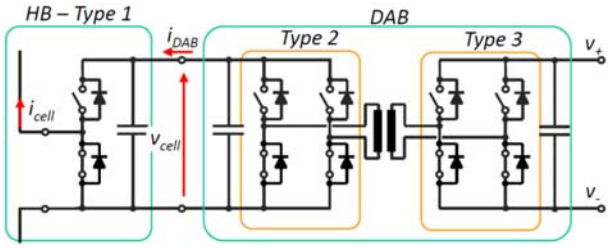

Fig. 9.- MMC cell and DAB for the MMC-based PET

CHB and MMC-based PETs

One of the most widely studied configurations for the three-stage PET in Fig. 1 is derived from the CHB topology, it is shown in Fig. 6, [9]-[11], [15]. A Dual Active Bridge (DAB) DC/DC converter is used to inject/drag power from the CHB cells. Fig. 7 shows a detailed representation of the CHB cell & DAB. The LV side of the DABs are parallelized to form a low-voltage, high current DC link. A conventional DC/AC three-phase power converter (controlled rectifier) is then used to provide the LVAC port. The CHB-based PET in Fig. 6 performs an AC/AC power conversion with galvanic isolation, similar to the LFT, but can also implement all the functionalities which are intrinsic to the CHB (reactive power and harmonic compensation, …), as well as control the power flow and avoid the propagation of disturbances between the HV and LV sides.

It is possible to extend the concept used in Fig. 6 to the case of the MMC, the resulting structure being shown in Fig. 8, [15], [16]. As in the CHB case, DABs are used to realize a bidirectional power transfer between the MMC cells and the LV side on the converter. Fig. 9 shows in detail the MMC cell & DAB. Other MMC-based configurations can be found in [21], [22].

The topology in Fig. 6 has two ports, performing an AC/AC transformation. On the other hand, the power converter in Fig. 8 has three ports: HVDC, high-voltage AC (HVAC) and low-voltage AC (LVAC). The HVDC link in the MMC-based implementation in Fig. 8 enables new functionalities compared to the power converter in Fig. 6, but this is at the price of a significant increase in the number of cells, and consequently of power devices, passives and auxiliary circuitry.

To illustrate the differences between the CHB and MMC-based topologies, the particular case of a PET connecting two AC grids of 24kV and 400V respectively is discussed. This is one of the configurations being considered within the SPEED project [39]. A cell voltage v_{cell} = 2 kV was selected, which is equal to the DAB voltage in the HV side. The DC link voltage in the LV side is 1 kV. The DABs are designed for rated power of 10 kW.

Number of cells

The peak-to-peak phase voltage of the HVAC is 39.2 kV. The number of cells required for the CHB implementation is given by (11), ceil standing for the next larger integer.

$$N_{CHB} = ceil\left(\frac{v_{phase\ peak}}{v_{cell}}\right) \tag{11}$$

The HVDC voltage for the MMC-based PET topology must be larger than this value, a HVDC of 40kV was selected. The HVAC to HVDC ratio without triplen harmonic injection in the AC voltage is R_{nothi} = 0.98. The minimum number of cells required for the MMC-based implementation is given by (12) assumed that triplen harmonic injection is not used. The minimum number of cells if triplen harmonic are used is obtained replacing 2 by √3 in the right side of (12). Discussion on the effects of triplen harmonic injection in the AC voltages of the MMC can be found in [40].

$$N_{MMC} = ceil\left(\frac{2 \cdot v_{dc}}{v_{cell}}\right) \tag{12}$$

Table I shows the main constructive characteristics for both implementations. It is observed that for the same HV side voltage, the MMC-based design requires four times the number of cells of the CHB-based design. However, the number of devices for the MMC case is only double than for the CHB case, as the second uses full-bridges while the first requires half-bridges. It is also worth to note that the power transferred between the HV and LV sides for the MMC-based implementation is four times the power of the CHB implementation. This is due to the fact that the DABs in both configurations have the same ratings, but the MMC-based PET uses four times the number of cells of the CHB case.

TABLE I: COMPARATIVE ANALYSIS OF CHB AND MMC TOPOLOGIES

	CHB-based PET	MMC-based PET
v_{acHV}/v_{acHV}	24 kV / 400 V (*phase-phase*, *rms*)	
V_{cell}	2 kV	
N_{leg}	10	40
N_{DAB}	30	120
P_{DAB}	10 kW	
P_{TOTAL}	300 kW	1200 kW
# devices*	120	240
$I_{cell\text{-}peak}/I_{DAB}$	√3	2+4√3

* Only CHB and MMC cells are considered. Does not include DABs power devices

Power devices requirements and HF transformer

There are significant differences in the requirements for the power devices in the circuits shown in Fig. 7 and Fig. 9. In the discussion following, *Type* 1 devices refers to the power devices in the FB and HB connecting the DABs with the high-voltage ports of the PETs. *Type* 2 and *Type* 3 devices refer to the devices in the HV and LV sides of the DAB respectively.

All the devices in the HV side withstand the same DC link voltage. Consequently, they should have the same (or similar) voltage rating albeit different commutation requirements and current ratings. Commutation requirements for *Type 1* devices in CHB and MMC cells are low due to their multilevel nature [18], [41]. In the limit, a switching frequency as low as the fundamental frequency can be achieved using staircase modulation, provided that the number of levels is large enough [42], [43]. Diodes in CHB and MMC cells must conduct for relatively long periods of time, free-wheeling diodes with low conduction losses are therefore preferred. Considering the DC link voltage of 2 kV and the commutation requirements, 3.3 kV Si IGBT, using either Si or SiC free-wheeling diodes, are an adequate solution.

To reduce the size and weight of the HF transformer, a high switching frequency (in the range of several tens kHz) is desired in the DAB. For the required DC link voltage and switching frequency, modern 3.3 kV SiC MOSFET, with a peak current of 15 A are good candidates for the *Type* 2 devices.

The operation of the DAB in nominal conditions provides zero voltage switching, which is needed to achieve high efficiency with high switching frequencies. A straightforward control method for the DAB is the phase-shift modulation (PSM). This requires a careful selection of the leakage inductance of the HF transformer. Too low values implies non-ZVS under low loads, while too large values can limit the maximum power [44]. This second case is more likely to occur due the isolation required between the primary and secondary sides of the HF transformer to guarantee galvanic isolation between the HV and LV sides of the PET. It is finally noted that, ideally, the ZVS range is not limited for the case of an input/output voltage ratio equal to one (both referred to the same side of the transformer). However, this is not necessarily true in practice due to the parasitic capacitances of the switches. The main parameters of the HT transformer are given in Table II, its design and construction being a challenging task [45].

TABLE II: HF TRANSFORMER PARAMETERS

Rated power	10 kW
switching frequency	50 kHz
leakage inductance	950 μH
DC link voltage HV side	2 kV
turns ratio	2:1
Prim.-to-second. isolation	24 kV

Core material	CF138

As PSM is used to control the power transfer between the HV and LV sides of the DABs, identical switching characteristics are desired for *Type* 2 and *Type* 3 power devices. Since the voltage in the LVDC link is half of the voltage in the HV side, *Type* 3 devices should be rated for around half the voltage and twice the current of *Type* 2 devices, 1.7 kV SiC MOSFET being adequate. Synchronous rectification can be used, meaning that the requirements for the diodes are low, the MOSFET body diode can be enough.

All the power transferred by the DAB must be delivered by the FB (13) (losses neglected). The relationship between the peak current for *Type 1* (FB) and *Type 2* (DAB) devices for the CHB case is then given by (14).

$$P_{acLV} = P_{DAB\text{-}total} = -P_{acHV} \tag{13}$$

$$\frac{i_{cell\ peak}}{\bar{i}_{DAB}} = \sqrt{3} \tag{14}$$

It is noted that i_{cell} is an AC current at the grid frequency (50 or 60 Hz typically). On the contrary, i_{DAB} is a high frequency pulsated current, $\bar{i}_{DAB}$ being its average (DC) value, the DAB peak current can be roughly approached by $i_{DAB\ peak} \approx 1.3\,\bar{i}_{DAB}$.

Selection of the current ratings for the MMC-based PETs is not so straightforward. The multiport nature of this design opens new possibilities to split the power among the three ports, which affects to the current ratings of the power devices. Neglecting losses, the power balance in this case is given by (15)-(16).

$$P_{dcHV} + P_{acHV} + P_{DAB\text{-}total} = 0 \tag{15}$$

$$P_{DAB\text{-}total} = P_{acLV} \tag{16}$$

Fig. 10 shows the relationship between the MMC DC current i_{dc}, AC peak current $i_{a\ peak}$, and arm peak currents $i_{cell\ peak\ (\mathrm{MMC})}$, when the DAB is transferring its rated current, i.e. $P_{DAB\text{-}total}$ is at its rated value. The peak current for CHB-based PET cells $i_{cell\ peak\ (\mathrm{CHB})}$ is shown for reference. Minimum current in the *Type* 1 devices is obtained for $P_{dcHV}/P_{DAB\text{-}total} = -1$, i.e. the power injected by the DAB being entirely delivered to the DC port of the MMC. For $P_{dcHV}/P_{DAB\text{-}total} = 0$, all the power injected by the DABs is delivered to the AC port. In all the other cases, the power injected by the cells is split

between the AC and DC ports of the MMC. Control strategies to achieve this are discussed in a further section dealing specifically with MMC-based PET control.

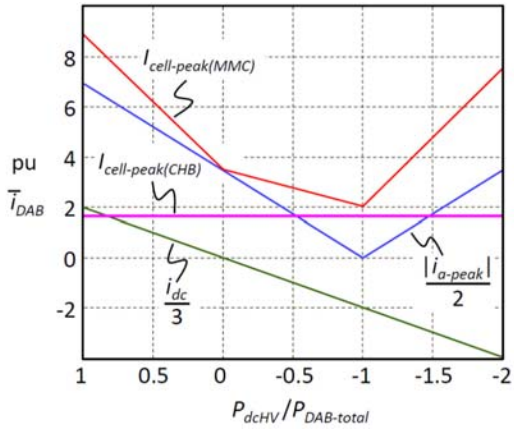

Fig. 10.- Peak current of the MMC-based and CHB-based PETs, as a function of P_{dcHV} / $P_{DAB\text{-}total}$. $P_{DAB\text{-}total}$ is constant and equal to its rated value. Currents are shown in pu of the DAB average current.

Table III summarizes the requirements for the power devices in the MMC design.

TABLE III: REQUIREMENTS FOR THE POWER SWITCHES

	Type 1	*Type 2*
Switching frequency	×100 Hz	×10 kHz
Transistor current	×10	×1
Diode current	Large	small (dead-time)

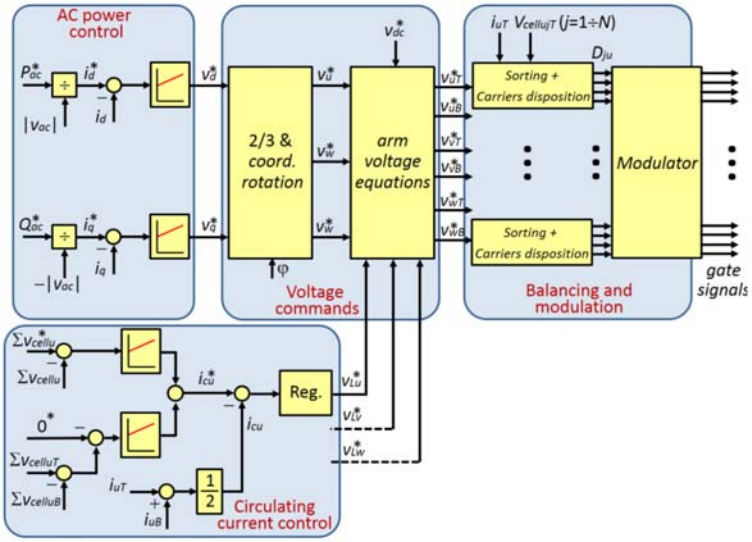

Fig. 11.- Schematic representation of the MMC control.

MMC control

Control of the MMC involves multiple objectives, which must be satisfied simultaneously. The control must maintain all the cell capacitors at their target voltage. This implies to match the power of the MMC AC and DC ports. Additional control targets can include minimization of the switching losses, minimization of the cell capacitors voltage ripple or minimization of the harmonic content of the circulating current [46], [47], [33]. Unfortunately, some of these targets are conflicting and must be therefore traded-off. There is a wide literature on MMC control strategies [23], [26], [27], [31]-[34], detailed discussion of this topic is beyond the scope of this paper. To illustrate the difficulty of the control, a potential implementation is shown in Fig. 11. The AC power references are transformed into d- and q-axis current references, synchronous PI current regulators being used to obtain the required AC voltages (*AC power control* block). The *circulating current control* block matches the DC and AC ports power by controlling the circulating current trough the top and bottom arm voltages. Arm voltages are then transformed into cell voltages. Modulation of the commanded cell voltages must be combined with a sorting algorithm to avoid imbalances among the capacitor voltages [23], [24], [34]. This is done by the *balancing and modulation* block in Fig. 11.

MMC-based PET control

Different approaches can be considered for the control of the CHB-based and MMC-based PETs in Fig. 6 and Fig. 8. If the voltage in the ports is established externally (i.e. by the grid), then a *grid feeding* strategy can be used. The power transferred by the port is controlled in this case. On the contrary, if the voltage in a port must be established by the PET, a *grid forming* strategy is needed. The target of the control in this case is to maintain the desired voltage. Since the power transferred is not controlled, some inner control loop is needed to guarantee that the current limits of the converter are not surpassed. It is not possible to configure all the ports in the *grid forming* mode, as the power balance cannot be guaranteed in this case. Consequently, at least one port must be configured in the *grid feeding* mode. Independent of the strategy being implemented, the control must always maintain the internal capacitor voltages at their target value.

As an example, two different control strategies for the MMC-based PET are briefly described following. In the first case (Fig. 12), all the three ports are configured in the *grid-feeding* mode. This means that there is full control on the power transfer among ports. In the second case (Fig. 13), LVAC port is configured in the *grid-forming* mode.

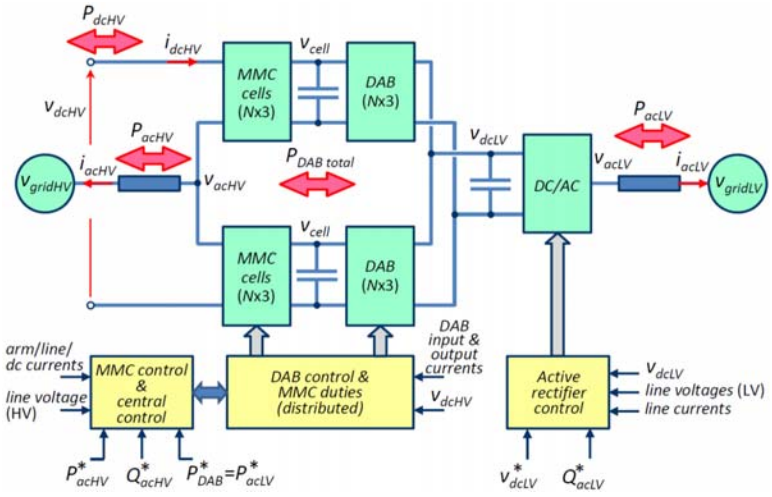

Fig. 12.- Schematic representation of a *grid feeding* control structure of a MMC-based multiport power converter. Variables with superscript * indicate commanded values.

MMC-based PET with grid-feeding configuration

This configuration is shown in Fig. 12. All the PET terminal voltages (v_{acHV}, v_{dcHV} and v_{acLV}) are already present. The LVAC ($P^*_{DAB} = P^*_{acLV}$) and HVAC (P^*_{acHV}) powers are commanded values, the central control regulating P_{dcHV} to match the power equation. The control is seen to consist of three major blocks:

- MMC. It is a centralized control [48]. It implements the normal functionalities, i.e. control of the HVAC and HVDC ports currents, as well as of the cell capacitor voltages v_{cell} [26], [27], [35]-[41].
- DABs. It is advantageous to distribute the DAB control in each cell, as the DABs operate independently (even if they all receive the same power command) and at much higher switching rates than the MMC cells [48]. The DABs connect two ports of constant (controlled) voltages, v_{cell} and v_{dcLV}, operating therefore as a current source.
- DC/AC converter in the LV side. It operates as a conventional controlled rectifier [49]. Commanded values for the active rectifier are the DC link voltage v^*_{dcLV} and the reactive power Q^*_{acLV}. The control will match P_{acLV} with $P_{DAB\text{-}total}$ through the d–axis component of i_{acLV}, which is required to maintain the DC link voltage v_{dcLV} at its target value.

Fig. 13 shows the response of the control strategy in Fig. 12. Commanded values are P_{acHV} and P_{DAB}. The MMC is enabled at t=10 ms, the active power command being 100 kW (Fig. 13-a). Initially the DABs are not transferring power, the power in the DC link of the MMC (Fig. 13-b) matching

therefore the AC power plus the converter losses. At t=0.3 s, the DABs are commanded to transfer a total amount of 40 kW, which is supplied by the controlled rectifier in the LV side (Fig. 13-d). To keep the power balance, the power supplied by the DC bus of the MMC is decreased in the same amount. The active power in the controlled rectifier and the power in the DC link of the MMC are internally controlled to balance the power.

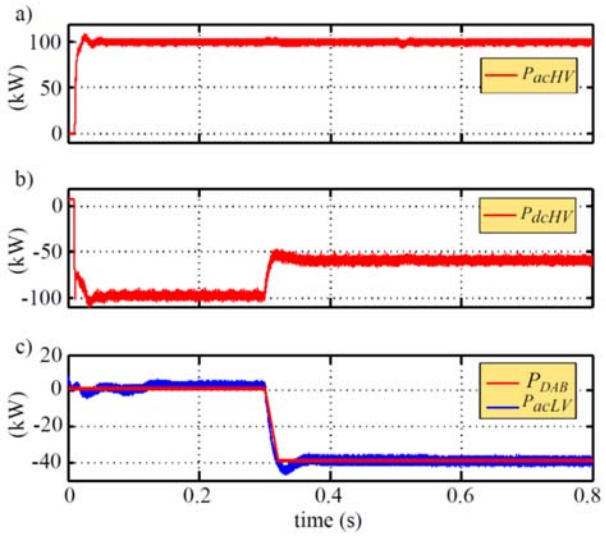

Fig. 13.- Simulation results. MMC-based multiport power converter with grid—feeding control. If the power has positive values, it flows from the PET port to the grid, while if it has negative values, it flows from the grid to the PET port. a) Active power in HVAC port; b) power in the HVDC port; c) total power injected by the DABs and active power in the LVAC port

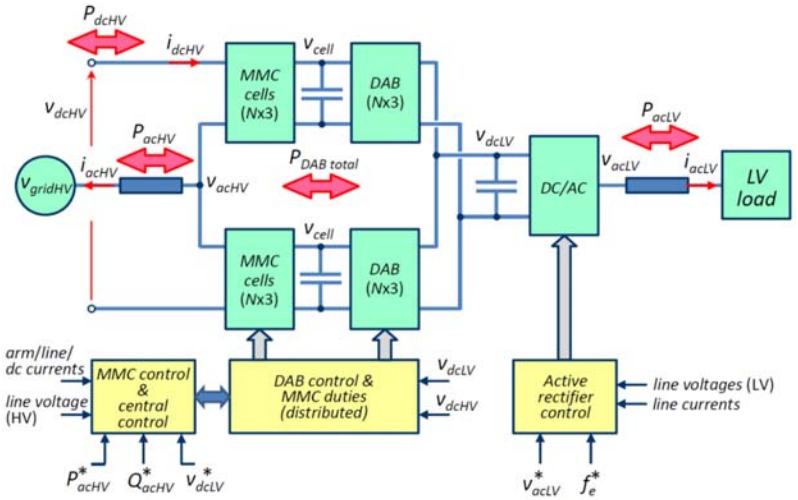

Fig. 14.- Schematic representation of a LV side *grid forming* control structure of a MMC based multiport power converter. Variables with superscript * indicate commanded values.

MMC-based PET with grid-forming configuration

This configuration is shown in Fig. 14. The MMC-based PET must provide in this case a voltage reference in the LV AC side, v_{acLV}. Major control blocks are the same as in the case of the grid-feeding configuration in Fig. 12, still some relevant differences exist:

- DAB. It now regulates the LVDC bus v_{dcLV}. The corresponding command is received from the central control unit.
- DC/AC converter in the LV side. It is now controlled to create the LVAC grid. The corresponding commands for the magnitude $\left|v_{acLV}^{*}\right|$ and frequency f_e^* of the LV grid are received from the central control.

Uses of MMC-based multiport power converter

Potential applications of the MMC-based topologies would be those requiring a multiport power conversion with medium/high voltage DC and AC ports. The configuration shown in Fig. 8 provides three ports: HVDC, HVAC and LVAC. It is noted however that with relatively minor modifications other configurations can be obtained in the LV side. Two different uses of the MMC-based implementation are discussed following: integration of DER and/or energy storage at the cell level and its use in vessels.

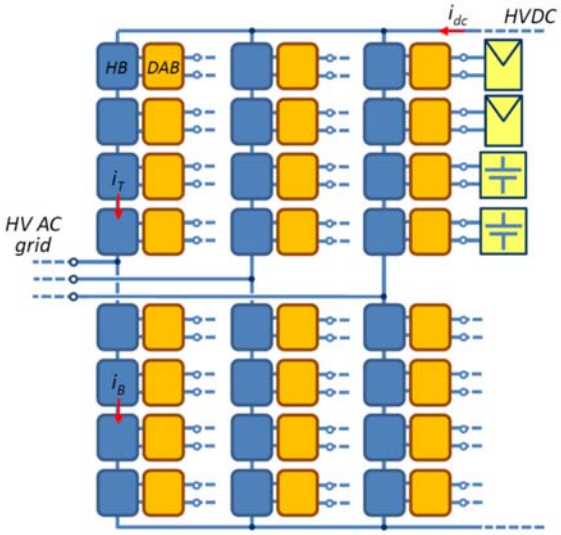

Fig. 15.- DER and/or energy storage integration in an MMC

DER and storage integration

In the configuration shown in Fig. 8, all the MMC cells are parallelized via DABs to form a full power-low voltage DC bus. It is possible however to connect elements to the DC link of the cells, e.g. energy storage [13] or distributed energy resources (DER) [14], as shown in Fig. 15. The

converter connecting the DER/energy storage to the MMC cell does not have to be necessarily a DAB, but can be optimized instead for the specific needs (galvanic isolation, bidirectional power flow, …).

One concern for the configuration shown in Fig. 15 are imbalances in the power being transferred by each cell of the MMC. Existing control methods for MMCs assume that all the cells have identical design and operate identically, meaning that both DC and AC components of the overall voltages in (7) are evenly split among cells. However, imbalances in the power transferred by the cells (e.g. due to panels receiving different solar radiation, or batteries operating with different states of charge) will necessarily result in imbalances among the cell voltages, as the current is common to all the cells in each arm. This is illustrated using the MMC-based PET prototype shown in Fig. 16. Fig. 17 shows the wave shapes for the MMC AC port and the DC link voltage of two cells during normal (balanced) operation. Fig. 18-left shows the DC component and the magnitude and phase of the AC (50 Hz) component of the cells voltage for the top arm, both for the case when the cells do not transfer power (conventional MMC) and when one cell per arm transfers power. Bottom arm behaves similarly and is not shown. The power transferred by the cells P_{cell} is 20% of the AC power P_{ac}. The imbalance in the power transferred by the MMC cells is seen to produce an imbalance in the cells voltages. Fig. 18-right shows the power in the DC and AC sides of the MMC, as well as the power transferred by the cells. The MMC is controlled to maintain constant the power in the AC side, meaning that power transferred by the cells is reflected in the power in the DC side of the converter.

a) MMC front view

b) MMC cell (HB, left) and DAB (right), including the HF transformer

Fig. 16.- Down-scaled prototype with four cells per arm

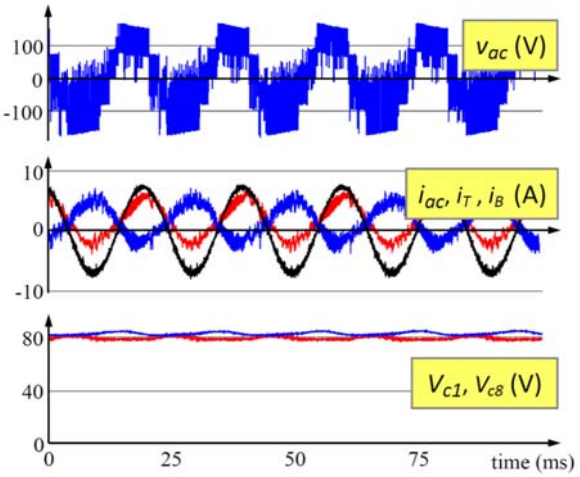

Fig. 17.- Experimental results. Top: AC output voltage of the MMC; Mid: top-arm, bottom-arm and AC output current of the MMC; Bottom – DC link voltage for cells 1 and 8.

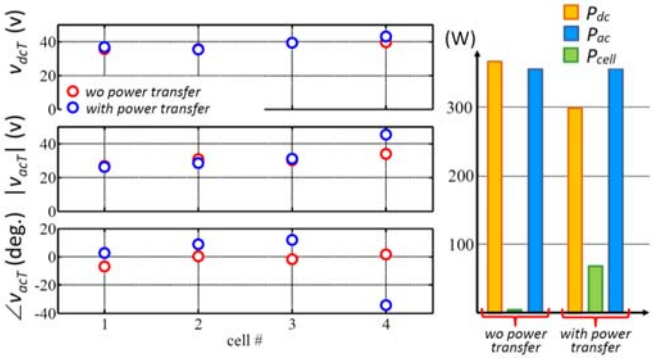

Fig. 18.- Experimental results. Left: DC and AC component of the cell voltage (only results for cells #1 to #4 shown); right: DC, AC and cells power without/with cell power transfer. P_{ac} remains constant when the cells transfer power.

Depending of the type asymmetry in the power (i.e. asymmetric among phases, arms or cells), different types of imbalances can occur in the cell voltages and in the HVAC port voltage [50], [51]. While in the case shown in Fig. 18 the system was stable, power imbalances can force to certain cells to reach their voltage limits. This will occur when the commanded voltage for a cell is <0 or >v_{cell}. If

this occurs controllability would be lost. Control strategies able to cope this situation should therefore be implemented if this condition is foreseen [51].

Use of the MMC-base multiport topology in vessels

Large vessels require complex electrical power systems, which must combine a large variety of main and auxiliary generation units, loads and storage systems, with powers that can go up to several tens MWs. The concept of Green Port aimed to reduce pollution when the vessel is at port, implies the integration of storage systems (e.g. batteries or flywheels) with their corresponding power converters. On shore power supply can be either low voltage (400-700 V) or medium voltage (6-11 kV).

Traditional Power Systems for large commercial vessels are characterized by a Medium Voltage AC (MVAC) distribution, which is supplied by diesel-generator sets. Medium Voltage DC (MVDC) is considered a promising technology to improve the power system performance [52], [53]. The IEEE Standard 1709 establishes 6, 12, 18, 24 and 30 kV as the preferred MV DC levels for future vessel designs [54]. Compared to MVAC distribution, MVDC has several well known advantages:

- No need for phase angle synchronization of sources thus simplifying connection and disconnection of different devices
- Reduction of the size and ratings of switchgear and cables and elimination of bulky low frequency transformers
- Improved fault management and system reconfiguration
- Elimination of reactive current
- Removal of frequency constraints from the design and operation of generator sets

Still AC distribution systems have two major advantages over the DC option:

- Conventional transformers require AC voltages
- Circuit breakers are dramatically less expensive for AC than for DC

Connection of such variety of sources and loads in a flexible, controllable and reliable manner requires the intensive use of electronic power converters. Fig. 19 shows a schematic representation of the future onboard grid based on MVDC [53], in which large generators (power by e.g. diesel engines or gas turbines) and propulsion motors coexists with a variety of distributed resources. The need of a MVDC link makes the MMC-based multilevel power converter a candidate able to cope with such requirements.

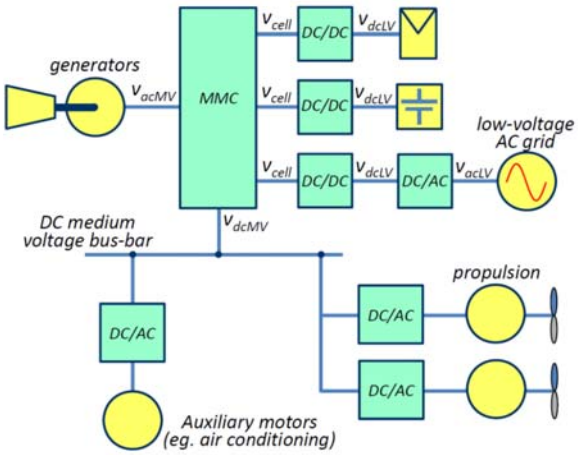

Fig. 19.- Schematic representation of an onboard architecture in vessels using an MMC-based multiport power converter with an MVDC link

Conclusions

CHBs are one of the most widely studied configurations for the three-stage power electronic transformers (PET). It is possible to extend the concept to MMC topology. The resulting MMC-based topology features multiport capabilities, intrinsically providing an HVDC port. However, to withstand the same voltage in the HV ports, MMC-based implementation requires four times the number of cells and double number of power devices compared to their CHB counterparts. Power devices requirements, modes of operation and control strategies have also been discussed. Examples of applications in which MMC-based multiport topologies can be advantageous include integration of low voltage DER and/or energy storage in HVDC systems, and power systems in vessels.

References.

[1] Ronan, E.R.; Sudhoff, S.D.; Glover, S.F.; Galloway, D.L., "A power electronic-based distribution transformer," in Power Delivery, IEEE Transactions on , vol.17, no.2, pp. 537-543, Apr 2002

[2] van der Merwe, J.W.; du T. Mouton, H.; , "The solid-state transformer concept: A new era in power distribution," AFRICON, 2009. AFRICON '09. , vol., no., pp. 1-6, 23-25 Sept. 2009

[3] Jih-Sheng Lai; Maitra, A.; Mansoor, A.; Goodman, F.; , "Multilevel intelligent universal transformer for medium voltage applications," Industry Applications Conference, 2005. Fourtieth IAS Annual Meeting. Conference Record of the 2005 , vol.3, no., pp. 1893-1899 Vol. 3, 2-6 Oct. 2005

[4] Xu She; Huang, A., "Solid state transformer in the future smart electrical system," in Power and Energy Society General Meeting (PES), 2013 IEEE, 21-25 July 2013

[5] J. Kolar and G. Ortiz, ”Solid-state-transformers: key components of future traction and smart grid systems,” in Proc. of the International Power Electronics Conference (IPEC), Hiroshima, Japan, 2014

[6] C. Zhao et al., "Power Electronic Traction Transformer—Medium Voltage Prototype," in IEEE Transactions on Industrial Electronics, vol. 61, no. 7, pp. 3257-3268, July 2014.

[7] M. Steiner and H. Reinold, "Medium frequency topology in railway applications," Power Electronics and Applications, 2007 European Conference on, Aalborg, 2007, pp. 1-10.

[8] Falcones, S.; Xiaolin Mao; Ayyanar, R., "Topology comparison for Solid State Transformer implementation," Power and Energy Society General Meeting, 2010 IEEE, 25-29 July 2010

[9] Advanced Power Converter for Universal and Flexible Power Management in Future Electricity Networks, UNIFLEX. FP6, EC Contract n: 019794 (SES6) EUROPEAN COMMISSION, DIRECTORATE J-ENERGY

[10] Zhao, T.; Wang, G.; Bhattacharya, S.; Huang, A. Q., "Voltage and Power Balance Control for a Cascaded H-Bridge Converter-Based Solid-State Transformer," Power Electronics, IEEE Transactions on , vol.28, no.4, pp. 1523-1532, April 2013

[11] Xu She; Lukic, S.; Huang, A.Q.; Bhattacharya, S.; Baran, M.; , "Performance evaluation of solid state transformer based microgrid in FREEDM systems," Applied Power Electronics Conference and Exposition (APEC), 2011 Twenty-Sixth Annual IEEE , vol., no., pp. 182-188, 6-11 March 2011

[12] Thomas Friedli, Johann W. Kolar, "Milestones in Matrix Converter Research", IEEJ Journal of Industry Applications, vol. 1, no. 1, pp.2-14, 2012.

[13] Vasiladiotis, M.; Rufer, A., "Analysis and Control of Modular Multilevel Converters With Integrated Battery Energy Storage," Power Electron., IEEE Trans. on , vol.30, no.1, pp. 163-175, Jan. 2015

[14] M. A. Perez, D. Arancibia, S. Kouro and J. Rodriguez, "Modular multilevel converter with integrated storage for solar photovoltaic applications," Industrial Electronics Society, IECON 2013 - 39th Annual Conference of the IEEE, Vienna, 2013, pp. 6993-6998.

[15] Shojaei, A.; Joos, G., "A topology for three-stage Solid State Transformer," in Power and Energy Society General Meeting (PES), 2013 IEEE, 21-25 July 2013

[16] Briz, F.; Lopez, M.; Rodriguez, A.; Zapico, A.; Arias, M.; Diaz- Reigosa, D., "MMC based SST," in Industrial Informatics (INDIN), 2015 IEEE 13th International Conference on , vol., no., pp. 1591-1598, 22-24 July 2015

[17] Kouro, S.; Malinowski, M.; Gopakumar, K.; Pou, J.; Franquelo, L.G.; Bin Wu; Rodriguez, J.; Perez, M.A.; Leon, J.I., "Recent Advances and Industrial Applications of Multilevel Converters," Industrial Electronics, IEEE Transactions on , vol.57, no.8, pp. 2553-2580, Aug. 2010

[18] Malinowski, M. , Gopakumar, K., Rodriguez, J., Perez, M.A., "A Survey on Cascaded Multilevel Inverters," Industrial Electronics, IEEE Transactions on , vol.57, no.7, pp. 2197-2206, July 2010

[19] B. Wu, High-Power Converters and AC Drives. New York: Wiley-IEEE Press, Mar. 2006.

[20] M. Glinka and R. Marquardt: A New AC/AC Multilevel Converter Family, IEEE Transactions on Industrial Electronics, vol. 52, no. 3, June 2005

[21] Y. Liu, A. Escobar-Mejía, C. Farnell, Y. Zhang, J. C. Balda and H. A. Mantooth, "Modular multilevel converter with high-frequency transformers for interfacing hybrid DC and AC microgrid systems," 2014 IEEE 5th International Symposium on Power Electronics for Distributed Generation Systems (PEDG), Galway, 2014, pp. 1-6.

[22] Zhu Haibin; Li Yaohua; Wang Ping; Li Zixin; Chu Zunfang, "Design of Power Electronic Transformer Based on Modular Multilevel Converter," Power and Energy Engineering Conference (APEC), 2012 Asia-Pacific, vol., no., pp.1,4, 27-29 March 2012

[23] A. Lesnicar, and R. Marquardt: An Innovative Modular Multilevel Converter Topology Suitable for a Wide Power Range, IEEE PowerTech Conference, Bologna, Italy, June 23-26, 2003

[24] A. Lesnicar, and R. Marquardt: A new modular voltage source inverter topology, EPE 2003, Toulouse, France, September 2-4, 2003

[25] Debnath, S.; Jiangchao Qin; Bahrani, B.; Saeedifard, M.; Barbosa, P., "Operation, Control, and Applications of the Modular Multilevel Converter: A Review," Power Electronics, IEEE Transactions on , vol.30, no.1, pp. 37-53, Jan. 2015

[26] Hagiwara, M.; Akagi, H.; , "Control and Experiment of Pulsewidth- Modulated Modular Multilevel Converters," IEEE Trans. Power Elec., , vol.24, no.7, pp. 1737-1746, July 2009

[27] Antonopoulos, A.; Angquist, L.; Nee, H.-P.; , "On dynamics and voltage control of the Modular Multilevel Converter," Power Electronics and Applications, 2009. EPE '09. 13th European Conference on, pp. 1-10, 8-10 Sept. 2009

[28] Rohner, S.; Bernet, S.; Hiller, M.; Sommer, R.; , "Analysis and Simulation of a 6 kV, 6 MVA Modular Multilevel Converter," IECON'09, pp.225-230, 3-5 Nov. 2009, Porto, PT

[29] Akagi, H., "Classification, Terminology, and Application of the Modular Multilevel Cascade Converter (MMCC)," Power Electron., IEEE Trans. on , vol.26, no.11, pp. 3119-3130, Nov. 2011

[30] Hagiwara, M.; Maeda, R.; Akagi, H.; , ”Control and Analysis of the Modular Multilevel Cascade Converter Based on Double-Star Chopper- Cells (MMCC-DSCC),” Power Electron., IEEE Trans. on , vol.26, no.6, pp. 1649-1658, June 2011

[31] Li, Wei; Gregoire, Luc-Andre; Belanger, Jean., ”Control and Performance of a Modular Multilevel Converter System”, Conference on Power Systems (CIGRE), Canada, 6-8 Sept. 2011

[32] Perez, M.A.; Lizana F, R.; Rodriguez, J., ”Decoupled current control of modular multilevel converter for HVDC applications,” IEEE ISIE’12, pp. 1979-1984, 28-31 May 2012, Hangzhou, CHN

[33] Jae-Jung Jung; Hak-Jun Lee; Seung-Ki Sul, ”Control strategy for improved dynamic performance of variable-speed drives with the Modular Multilevel Converter,” IEEE ECCE’13, pp. 1481-1488, 15-19 Sept. 2013, Denver, CO, USA

[34] Saeedifard, M.; Iravani, R., ”Dynamic Performance of a Modular Multilevel Back-to-Back HVDC System,” Power Delivery, IEEE Trans. on , vol.25, no.4, pp. 2903,2912, Oct. 2010

[35] Gum Tae Son; Hee-Jin Lee; Tae Sik Nam; Yong-Ho Chung; Uk-Hwa Lee; Seung-Taek Baek; Kyeon Hur; Jung-Wook Park, ”Design and Control of a Modular Multilevel HVDC Converter With Redundant Power Modules for Noninterruptible Energy Transfer,” Power Delivery, IEEE Transactions on , vol.27, no.3, pp. 1611-1619, July 2012

[36] Huber, J.E.; Kolar, J.W., ”Optimum number of cascaded cells for high-power medium-voltage multilevel converters,” Energy Conversion Congress and Exposition (ECCE), 2013 IEEE , vol., no., pp. 359-366, 15-19 Sept. 2013

[37] L. Baruschka and A. Mertens, "Comparison of Cascaded H-Bridge and Modular Multilevel Converters for BESS application," 2011 IEEE Energy Conversion Congress and Exposition, Phoenix, AZ, 2011, pp. 909-916.

[38] A. Marzoughi, R. Burgos, D. Boroyevich and Y. Xue, "Investigation and comparison of cascaded H-bridge and modular multilevel converter topologies for medium-voltage drive application," IECON 2014 - 40th Annual Conference of the IEEE Industrial Electronics Society, Dallas, TX, 2014, pp. 1562-1568.

[39] “Silicon Carbide Power Technology for Energy Efficient Devices (SPEED)”, Ref. FP7-NMP3-LA-2013-604057, EU – FP7, Large Scale Integrating Collaborative Research Project.

[40] R. Li; J. Fletcher; L. Xu; B. Williams, "Enhanced Flat-Topped Modulation for MMC Control in HVDC Transmission Systems," in IEEE Transactions on Power Delivery, to be published in 2016, pre-print available through IEEE Xplore

[41] J. Rodriguez, J.-S. Lai, and F. Z. Peng, ”Multilevel inverters: A survey of topologies, controls, and applications,” IEEE Trans. Ind. Electron., vol. 49, no. 4, pp. 724-738, Aug. 2002.

[42] Ke Shen; Chuang Liu; Jianze Wang; Xingguo Cai; Yanchao Ji, "A stochastic optimal approach for fundamental frequency modulated modular multilevel converter," in Power and Energy Society General Meeting, 2012 IEEE, 22-26 July 2012

[43] Ilves, K.; Antonopoulos, A.; Norrga, Staffan; Nee, H.-P., "A New Modulation Method for the Modular Multilevel Converter Allowing Fundamental Switching Frequency," in Power Electronics, IEEE Transactions on , vol.27, no.8, pp. 3482-3494, Aug. 2012

[44] Rodriguez, A.; Vazquez, A.; Lamar, D.G.; Hernando, M.M.; Sebastian, J., "Different Purpose Design Strategies and Techniques to Improve the Performance of a Dual Active Bridge With Phase-Shift Control," Power Electronics, IEEE Transactions on , vol.30, no.2, pp. 790-804, Feb. 2015.

[45] Mario Lopez, Fernando Briz, Mariam Saeed, Manuel Arias and Alberto Rodriguez, "Comparative Analysis of Modular Multiport Power Electronic Transformer Topologies", accepted for the 8th Annual IEEE Energy Conversion Congress & Exposition (ECCE), 18-23 September 2016, Milwaukee, US

[46] Picas, R.; Pou, J.; Ceballos, S.; Agelidis, V. G.; Saeedifard, M., ”Minimization of the capacitor voltage fluctuations of a modular multilevel converter by circulating current control,” IECON 2012 - 38th Annual Conference on IEEE Industrial Electronics Society, pp. 4985-4991, 25-28 Oct. 2012

[47] Qingrui Tu; Zheng Xu; Jing Zhang, ”Circulating current suppressing controller in modular multilevel converter,” IECON 2010 - 36th Annual Conference on IEEE Industrial Electronics Society, pp. 3198-3202, 7-10 Nov. 2010

[48] Lopez, M.; Rodriguez, A.; Blanco, E.; Saeed, M.; Martinez, A.; Briz, F., ”Design and implementation of the control of an MMC-based solid state transformer,” in Industrial Informatics (INDIN), 2015 IEEE 13th International Conference on, pp. 1583-1590, 22-24 July 2015

[49] Muhammad H. Rashid, Power Electronics Handbook, Academic Press, 2001

[50] Briz, F.; Lopez, M.; Zapico, A.; Rodriguez, A.; Diaz-Reigosa, D., ”Operation and Control of MMCs Using Cells with Power Transfer Capability,” IEEE APEC’15, 15-19 March 2015, Charlotte, NC, USA

[51] Lopez, M.; Briz, F.; Zapico, A.; Rodriguez, A.; Diaz-Reigosa, D., ”Control strategies for MMC using cells with power transfer capability,” in Energy Conversion Congress and Exposition (ECCE), 2015 IEEE , vol., no., pp. 3570-3577, 20-24 Sept. 2015

[52] S. Castellan, R. Menis, A. Tessarolo, and G. Sulligoi, “Power electronics for all-electric ships with MVDC power distribution system: An overview,” in Ecological Vehicles and Renewable Energies (EVER), 2014 Ninth International Conference on, IEEE, 2014.

[53] F. D. Kanellos, J. Prousalidis, and G. J. Tsekouras, “Onboard DC grid employing smart grid technology: challenges, state of the art and future prospects,” IET Electrical Systems in Transportation, vol. 5, pp. 1–11, Mar. 2015.

[54] Institute of Electrical and Electronics Engineers and IEEE-SA Standards Board, IEEE recommended practice for 1 kV to 35 kV medium-voltage DC power systems on ships. New York: Institute of Electrical and Electronics Engineers, 2010.